





**Relating fragile-to-strong transition to fragile glass via lattice model simulations**Chin-Yuan Ong <sup>1</sup>, Chun-Shing Lee <sup>2,1</sup>, Xin-Yuan Gao <sup>1</sup>, Qiang Zhai,<sup>3</sup> Zhenhao Yu <sup>4</sup>, Rui Shi,<sup>4</sup>  
Hai-Yao Deng,<sup>5,\*</sup> and Chi-Hang Lam<sup>1,†</sup><sup>1</sup>*Department of Applied Physics, Hong Kong Polytechnic University, Hong Kong, China*<sup>2</sup>*School of Science, Harbin Institute of Technology (Shenzhen), Shenzhen 518055, China*<sup>3</sup>*School of Physics, MOE Key Laboratory for Nonequilibrium Synthesis and Modulation of Condensed Matter, Xi'an Jiaotong University, Xi'an 710049, China*<sup>4</sup>*Zhejiang Key Laboratory of Micro-nano Quantum Chips and Quantum Control, School of Physics, Zhejiang University, Hangzhou 310027, China*<sup>5</sup>*School of Physics and Astronomy, Cardiff University, 5 The Parade, Cardiff CF24 3AA, Wales, United Kingdom*

(Received 1 August 2023; accepted 11 April 2024; published 23 May 2024)

Glass formers are, in general, classified as strong or fragile depending on whether their relaxation rates follow Arrhenius or super-Arrhenius temperature dependence. There are, however, notable exceptions, such as water, which exhibit a fragile-to-strong (FTS) transition and behave as fragile and strong, respectively, at high and low temperatures. In this work, the FTS transition is studied using a distinguishable-particle lattice model previously demonstrated to be capable of simulating both strong and fragile glasses [C.-S. Lee, M. Lulli, L.-H. Zhang, H.-Y. Deng, and C.-H. Lam, *Phys. Rev. Lett.* **125**, 265703 (2020)]. Starting with a bimodal pair-interaction distribution appropriate for fragile glasses, we show that by narrowing down the energy dispersion in the low-energy component of the distribution, a FTS transition is observed. The transition occurs at a temperature at which the stretching exponent of the relaxation is minimized, in agreement with previous molecular dynamics simulations.

DOI: [10.1103/PhysRevE.109.054124](https://doi.org/10.1103/PhysRevE.109.054124)**I. INTRODUCTION**

Glasses are produced when liquids are supercooled below the glass transition temperature  $T_g$  [1–3]. Depending on how dramatically the relaxation rate of a glass changes with respect to the temperature upon cooling, it is then classified as a strong glass or a fragile glass. For strong glass, the dynamics follows the Arrhenius law. In contrast, it shows a super-Arrhenius temperature dependence for fragile glass. However, there exist many types of liquids that do not obey this classification, such as water [4,5], silica [6],  $\text{BeF}_2$  [7], and some metallic glasses [8]. They are fragile at high temperature, but their dynamics obeys the Arrhenius law characteristic of strong glass at low temperature. This anomaly is known as the fragile-to-strong (FTS) transition.

Water is the most widely studied material exhibiting a FTS transition. Several hypotheses based on mode-coupling theory [9] and Adam-Gibbs theory [4] have been proposed to account for the phenomenon. Subsequently, Stanley and co-workers explained the dynamic abnormalities with a crossover from a high-density liquid to a low-density one at a line which is known as the Widom line [10]. It is defined as the maxima of thermodynamics response functions that emanate from a proposed liquid-liquid critical point.

Recently, Tanaka and coworkers developed a hierarchical two-state model that describes the structural, thermodynamic, and dynamic properties of liquid water in a unified manner [11–14]. In this model, the “apparent” fragile-to-strong transition is interpreted as a crossover between two Arrhenius behaviors with different activation energies for two types of local structures that coexist in liquid water [15,16]. This model predicts the maximization of dynamic fluctuations upon cooling at a crossover temperature below the Widom line [11–14]. The existence of two types of local structures and the maximization of dynamic fluctuations in liquid water have been confirmed in TIP4P/2005 [13,14], TIP5P [11,12], and ST2 [11,12] water models and supported by experimental measurements [13,14,17–21]. Molecular dynamics (MD) simulations of other supercooled liquids with two distinct groups of interactions have also demonstrated a fragile-to-strong transition [22,23].

In this paper, we study the FTS transition using the distinguishable-particle lattice model (DPLM) of glass [24]. The DPLM has recently been applied successfully to address Kovacs’ expansion gap paradox [25], the connection between fragility and thermodynamics quantities [26], the heat capacity hysteresis in cooling-heating cycles with large overshoots in fragile glasses [27], two-level systems at low temperature [28], and a diffusion-coefficient power law under a particle partial-swap algorithm [29]. We show that materials exhibiting a high fragility and a FTS transition are closely related and can differ only in the low-energy statistics of the particle pair interactions. Specifically, by simply altering the low-energy

\*dengh4@cardiff.ac.uk

†C.H.Lam@polyu.edu.hk

component of a pair-interaction energy distribution adopted in the DPLM, a fragile glass model can be turned into a system exhibiting a FTS transition.

The DPLM is a lattice gas model defined on a two-dimensional (2D) square lattice with  $N$  distinguishable particles [24–29]. Periodic boundary conditions are assumed. At most one particle can occupy a site at a time. Voids of a density,  $\phi_v$ , are introduced in the system as unoccupied sites. The total energy of the system is defined as

$$E = \sum_{\langle i,j \rangle} V_{s_i s_j}, \quad (1)$$

where the sum is over occupied nearest-neighbor sites  $i$  and  $j$ , and the particle index  $s_i = 1, \dots, N$  represents which particle is located at site  $i$ . The interaction energy  $V_{kl}$  between particles  $k$  and  $l$  is randomly sampled from a pair-interaction distribution,  $g(V)$ , before the simulation commences. The DPLM can produce both strong and fragile glasses by implementing a uniform-plus-delta bimodal interaction distribution given by [26]

$$g(V) = \frac{G_0}{\Delta V} + (1 - G_0)\delta(V - V_1), \quad (2)$$

for  $V_0 \leq V \leq V_1$ , with  $\Delta V = V_1 - V_0$ . The thermodynamic parameter  $G_0$  obeys  $0 < G_0 \leq 1$ . Strong and fragile glasses correspond to large and small  $G_0$ , respectively.

The system follows void-induced dynamics governed by the Metropolis algorithm. Specifically, each particle can hop to an unoccupied nearest-neighbor site at temperature  $T$  at a rate of

$$w = w_0 \exp\left[-\frac{E_0 + \theta(\Delta E) \Delta E}{k_B T}\right], \quad (3)$$

where  $\Delta E$  represents the change in total energy  $E$  of the system after hopping,  $k_B = 1$  is the Boltzmann constant,  $\theta$  denotes the Heaviside step function,  $E_0$  is an energy barrier offset, and  $w_0$  is a rate constant.

## II. FRAGILE-TO-STONG TRANSITION

Dynamic behaviors of the DPLM largely depend on the pair-interaction distribution  $g(V)$ . To enable a fragile-to-strong transition, the uniform-plus-delta distribution in Eq. (2) is replaced in our main simulations in this work by a bi-delta distribution,

$$g(V) = G_1\delta(V - V_0) + (1 - G_1)\delta(V - V_1), \quad (4)$$

where  $V_0$  and  $V_1$  ( $V_0 < V_1$ ) are the two possible interaction energies. The thermodynamic parameter  $G_1$ , analogous to  $G_0$  in Eq. (2), represents the probabilistic weight of the lower interaction energy  $V_0$ . We take  $V_0 = 0$  and  $V_1 = 1$  so that  $\Delta V = V_1 - V_0 = 1$ .

We have performed kinetic Monte Carlo simulations in 2D on a square lattice of length  $L = 100$  with the bi-delta pair interaction in Eq. (4). We take  $\phi_v = 0.01$ ,  $E_0 = 0.5$ , and  $w_0 = 10^6$ . The diffusion coefficient  $D$  at various temperatures  $T$  is measured (see the Appendix for details). The value of  $\phi_v$  considered here is similar to those in our previous studies [24,26] and it allows our simulations to reproduce features of interest within practical runtimes. In principle, voids may

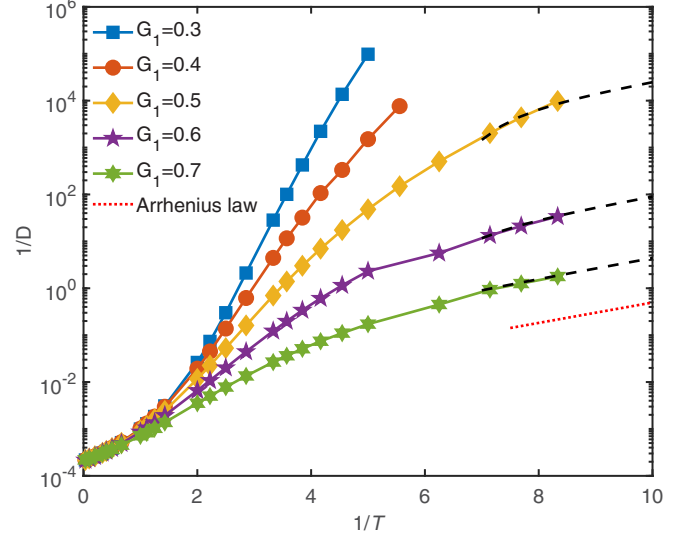


FIG. 1. Inverse particle diffusion coefficient  $\log_{10}(1/D)$  against inverse temperature  $1/T$  for various probabilistic weights  $G_1$  of the low-energy state. We put  $E_0 = 0.5$  and  $w_0 = 10^6$ . The dashed lines represent fits to Eq. (7). The dotted line following Eq. (6) is a guide to the eye.

take a more general form called quasivooids and their density  $\phi_v$  can be inferred from particle trajectories in colloidal glass experiments [30]. For molecular glasses in which particle trajectories cannot be resolved, appropriate values of  $\phi_v$  can only be justified in the future by comparing macroscopic dynamical quantities such as particle diffusion coefficients obtained from DPLM simulations or theoretical calculations [31] with those from experiments. Figure 1 shows an Arrhenius plot of  $1/D$  for various values of  $G_1$ . For the smallest value of  $G_1 = 0.3$  reported, we observe for  $1/T \lesssim 4$  a curvature in the semi-log plot, indicating a super-Arrhenius temperature dependence of  $1/D$ . This signifies a high-temperature fragile regime and the result is qualitatively similar to previous simulations in Ref. [26] for moderately fragile glass with  $G_0 = 0.3$  using the uniform-plus-delta distribution in Eq. (2). Nevertheless, a distinct feature in Fig. 1 is that for  $1/T \gtrsim 4$  the super-Arrhenius behavior turns into a sub-Arrhenius one, which was not observed in Ref. [26]. The results are qualitatively similar for all other values of  $G_1$  reported, although the high-temperature super-Arrhenius nature diminishes at larger  $G_1$ .

The termination of the high-temperature super-Arrhenius behavior as temperature decreases marks a FTS transition. Far below the transition at very low temperature, the dynamics is Arrhenius as is typical of strong glass. As lattice models are often more tractable analytically, the low-temperature Arrhenius behavior can be proven easily as follows. For  $k_B T \ll \Delta V$ , excitation to interaction  $V_1$  is suppressed so that only the lower-energy interaction  $V_0$  is relevant. All possible particle hops are then constrained to those resulting at no energy change, i.e.,  $\Delta E = 0$ . The rate  $w$  of all energetically possible hops as given in Eq. (3) then follow the same Arrhenius rate:

$$w = w_0 \exp\left(-\frac{E_0}{k_B T}\right), \quad (5)$$

which defines the dynamic timescale. Simulations at different low temperatures are thus similar except for this trivial scaling factor in the hopping rate. We therefore arrive at the low-temperature Arrhenius form

$$D \sim \exp\left(-\frac{E_0}{k_B T}\right). \quad (6)$$

The result signifies a strong behavior.

We observe from Fig. 1 that the Arrhenius behavior in Eq. (6) is directly verified at low temperature for  $G_1 = 0.7$ . For larger  $G_1$ , the observed trend is also consistent with a convergence to Eq. (6). When approaching the Arrhenius regime, we find that  $D$  follows the empirical form

$$D = D_0 \exp\left[-\frac{E_0}{k_B T} + \left(\frac{c_1}{T} - c_2\right)^{-4}\right], \quad (7)$$

where  $D_0$ ,  $c_1$ , and  $c_2$  are constants and it reduces to Eq. (6) at low temperature. For example, for  $G_1 = 0.5$ , fitted values are  $D_0 = 181$ ,  $c_1 = 0.316$ , and  $c_2 = 1.30$ .

### III. MODELING WATERLIKE LIQUID

We have demonstrated in the previous section that, by adopting a different interaction distribution,  $g(V)$ , a model of fragile glass can be turned into one exhibiting a FTS transition. We now further generalize it to model waterlike liquid more closely. In water, both hydrogen and nonhydrogen bonds are present and they are crucial in studying its anomalies [32,33]. We envision that the two interaction energies  $V_0$  and  $V_1$  in Eq. (4) now describe hydrogen and nonhydrogen bonds, respectively, an interpretation in line with a two-state picture of water [12,13].

We consider the probabilistic weight  $G_1 = 0.38$  of the low-energy interaction  $V_0$ . This value allows simulations to be performed within a manageable runtime for observing both a high fragility at high temperature and a FTS transition at low temperature. The bottom curve in Fig. 2 shows  $1/D$  hence obtained. When compared with amorphous water, we notice however that, relative to the high-temperature regime, the temperature dependence of the dynamics at low temperature is rather weak, corresponding to an effective low-temperature energy barrier being too small. This issue can be attributed to the constant barrier offset  $E_0$  adopted in Eq. (3).

In molecular systems, barriers of particle motions depend on the precise molecular structures and, in particular, on the bond types. A higher barrier is expected for the hopping of particles participating in more hydrogen bonds. We thus generalize the model to include an additional bond-dependent barrier offset term. Consider particle  $k$  attempting to hop from site  $i$  to site  $j$ . Let  $\Omega_{ij}$  be the set of all other particles at any of the six nearest-neighboring sites of  $i$  and  $j$ . The rate in Eq. (3) is generalized to

$$w = w_0 \exp\left[-\frac{E_0 + \theta(\Delta E) \Delta E + U(k, \Omega_{ij})}{k_B T}\right]. \quad (8)$$

Here, we have included an additional hopping-energy barrier term  $U(k, \Omega_{ij})$  of magnitude  $U_0$  defined as

$$U(k, \Omega_{ij}) = \frac{U_0}{C} \sum_{l \in \{\Omega_{ij}\}} \delta(V_{kl}, V_0), \quad (9)$$

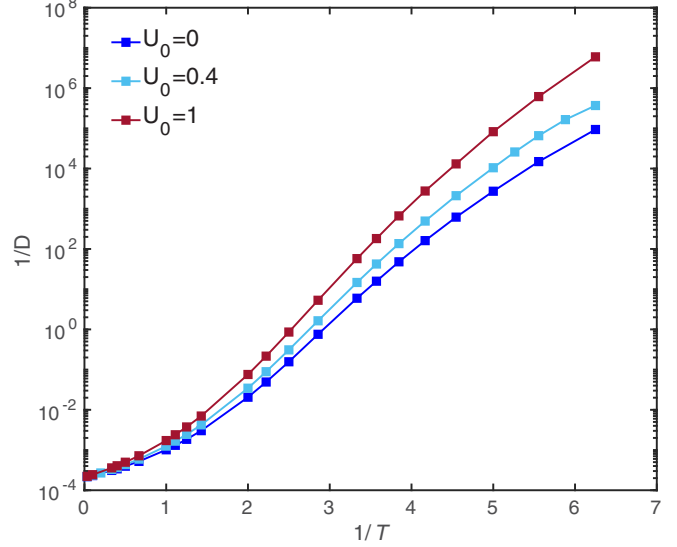


FIG. 2. Inverse particle diffusion coefficient  $1/D$  against inverse temperature  $1/T$  for various  $U_0$ . We use  $G_1 = 0.38$ ,  $E_0 = 0.5$ , and  $w_0 = 10^6$ .

where  $C = 6$  represents the number of bonds affected by the hop, including three to be deformed and three to be formed. If all of these six bonds are all hydrogen bonds, Eq. (9) gives  $U(k, \Omega_{ij}) = U_0$ . This occurs at low temperature. In the other extreme, if all are nonhydrogen bonds,  $U(k, \Omega_{ij}) = 0$ , which may happen at high temperature. Note that dynamics based on Eqs. (8) and (9) satisfies detailed balance due to the symmetry  $U(k, \Omega_{ij}) = U(k, \Omega_{ji})$  corresponding to the same barrier offset for forward and backward hops.

To illustrate the physical relevance of  $U_0$ , Fig. 2 also shows measured  $1/D$  for various values of  $U_0 \geq 0$ . It can be observed that a larger  $U_0$  leads to further slow down in the dynamics at low temperature, but it has relatively little effect on the dynamics at high temperature. Introducing  $U_0$  thus allows the fine-tuning of the effective activation energy at low and high temperatures independently.

To best reproduce dynamical features of waterlike liquid within reasonable computational requirements, we consider  $G_1 = 0.38$ ,  $U_0 = 0.4$ ,  $E_0 = 0$ , and  $w_0 = 10^4$ . Figure 3 shows a kinetic Angell plot of  $1/D$  against  $T_g/T$  thus obtained. Here, the glass transition temperature  $T_g$  is defined as the temperature at which  $1/D = 5 \times 10^4$ , close to the slowest dynamic rates at which simulations are still practical. We obtain  $T_g = 0.105$  after extrapolating our simulation data to lower temperatures using

$$D = D_0 \exp\left[-\frac{E_0 + U_0}{k_B T} + \left(\frac{c_1}{T} - c_2\right)^{-4}\right], \quad (10)$$

which is an empirical form generalized from Eq. (7). Note that  $D_0$  depends on  $U_0$  while  $c_1$  and  $c_2$  are independent of  $U_0$ . At low temperature, it reduces to

$$D \sim \exp\left(-\frac{E_0 + U_0}{k_B T}\right). \quad (11)$$

which generalizes Eq. (6). For comparison, we also simulate a model of fragile glass by adopting the uniform-plus-delta

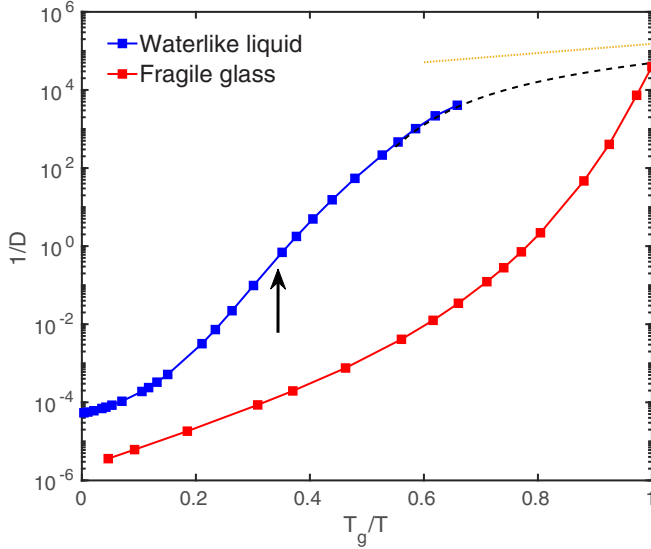


FIG. 3. Kinetic Angell plot for a model of waterlike liquid with a FTS transition and a fragile glass with  $T_g = 0.105$  and  $0.185$ , respectively. For the FTS transition case, the dashed line represents a fit to Eq. (10). The dotted line following Eq. (11) is a guide to the eye. The arrow points to temperature  $T = 0.35$  at which  $\beta$  is minimized.

interaction in Eq. (2) with  $G_0 = 0.03$ ,  $E_0 = 2.05$ ,  $w_0 = 10^6$ , and  $U_0 = 0$ . We get  $T_g = 0.185$ . Results have also been shown in Fig. 3. We have chosen the model parameters so that the respective features observed resemble qualitatively those of amorphous water and *o*-terphenyl, respectively, as reported in Ref. [12].

Nevertheless, we notice that the two characteristic turns in the Angell plot from our simulations are too stretched out. More precisely, the FTS transition temperature and the most super-Arrhenius point from Fig. 3 occur roughly at  $T_g/T \simeq 0.42$  and  $0.15$ , respectively, corresponding to a ratio of about 2.8. This is much larger than a ratio of roughly 1.5 from MD simulations [12]. We believe that the discrepancy may be due to a lack of correlation between neighboring bonds in our model, which is a feature of the DPLM [24] and interestingly is also assumed implicitly in two-state models [15,16,34].

Besides the diffusion coefficient, we have also measured the self-intermediate scattering function (see the Appendix). It follows the Kohlrausch-Williams-Watts (KWW) form characterized by the stretching exponent  $\beta$ . Figure 4 plots the temperature dependence of  $\beta$  obtained from the KWW fits. We observe a minimum of  $\beta$  at  $T \simeq 0.35$ . This value is consistent with the temperature at which the system starts to display the low-temperature Arrhenius behavior as seen in Fig. 3. Similar observations have been reported in molecular dynamics simulations of TIP4P/2005, TIP5P, and ST2 models of water with the minimum  $\beta$  (stretching exponent for the time correlation function of water dipole) associated with a maximized dynamic heterogeneity [11–13].

In addition, we have measured the four-point correlation function  $\chi_4$  which shows a peak at time  $\tau_4$  (see the Appendix). Figure 5 plots the peak height  $\chi_4(\tau_4)$  as a function of temperature. MD simulations in Refs. [11–13] show that  $\chi_4(\tau_4)$  exhibits a local maximum at the same temperature at which  $\beta$

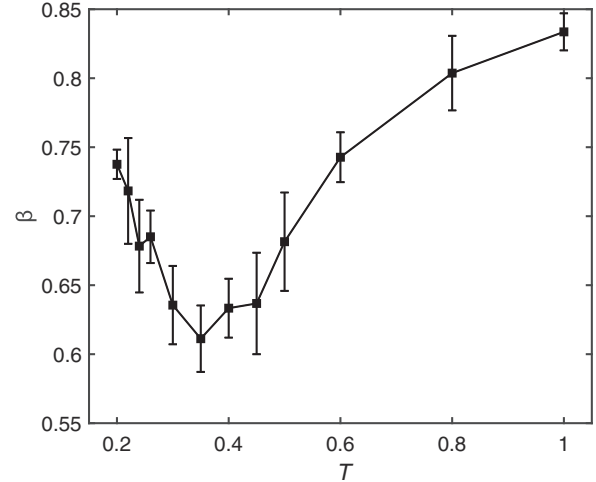


FIG. 4. Stretching exponent  $\beta$  plotted against  $T$  for the model of waterlike liquid.

is minimized. However, we observe from Fig. 5 no noticeable maximization at  $T \simeq 0.35$  at which  $\beta$  is minimized.

We remark that, while they both indicate dynamic heterogeneity, the stretching exponent  $\beta$  and the four-point correlation function  $\chi_4$  display distinct temperature dependencies in the simulations. As seen in Fig. 4, the temperature dependence of  $\beta$  is nonmonotonic: As the temperature drops,  $\beta$  first decreases from unity to a local minimum, where the FTS transition sets in, and then rises again as the temperature drops further. Nevertheless, as shown in Fig. 5, the peak height of  $\chi_4$  increases monotonically as the temperature drops. Such contrast manifests the fact that these quantities capture different aspects of dynamic heterogeneity. Namely,  $\beta$  mostly encrypts the heterogeneity of relaxation times, whereas  $\chi_4$  largely tells of the average correlation length of particle mobilities. This interpretation can be rationalized by the recently proposed configuration tree theory, which has successfully explained a variety of dynamical properties of the DPLM

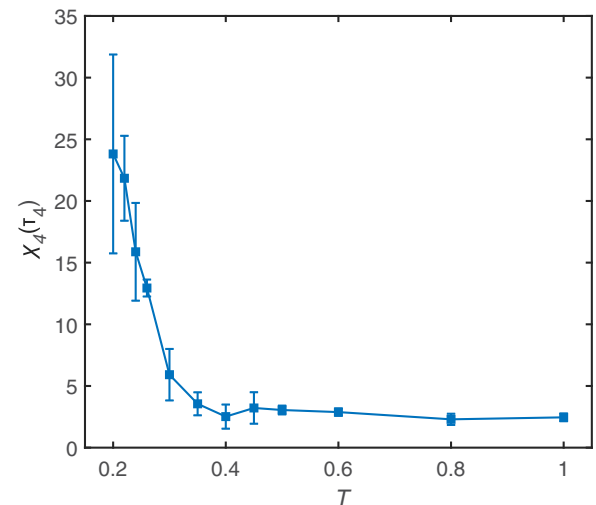


FIG. 5. Peak height  $\chi_4(\tau_4)$  of four-point correlation function plotted against  $T$  for the model of waterlike liquid.

[31,35]. According to this theory, structural relaxation occurs mainly due to the diffusion of mobile clusters, each consisting of a number of coupled (quasi-)voids signifying emergent dynamical facilitation. The number of voids required to make up each of these dominating clusters increases as temperature decreases. If mobile clusters of a range of sizes contribute to the structural relaxation,  $\beta$  tends to be small; otherwise it tends to unity. Meanwhile, the spatial correlation length of particle mobilities, as measured by the peak height of  $\chi_4$ , is principally set by the diffusion length of the cluster that freely diffuses the farthest without encountering another cluster. As the temperature drops, mobile clusters become fewer and diffuse further, hence a greater peak height of  $\chi_4$  and its monotonic increase. At temperatures far below the FTS transition, fluctuations are reduced because most interactions take the value  $V_0$ . The dynamics may then be dominated by clusters of one or a few particular sizes and hence  $\beta$  approaches towards unity. Around the transition, clusters of varying sizes contribute, leading to smaller  $\beta$ .

In Ref. [36], the emergence of the FTS transition has been found in MD simulations to be correlated to the temperature dependence of the average energy in the system. We now show that this correlation can also be observed in our simulations. The equilibrium average energy per particle  $\varepsilon = E/N$  in the DPLM has been derived in Ref. [24] and follows

$$\varepsilon = 2(1 - \phi_v)\bar{V}, \quad (12)$$

where the average interaction energy  $\bar{V}$  is given exactly in the thermodynamic limit by

$$\bar{V} = \int V p_{\text{eq}}(V) dV. \quad (13)$$

Here,  $p_{\text{eq}}(V)$  is the distribution of the interactions realized in an equilibrium system and follows

$$p_{\text{eq}}(V) = \frac{1}{\mathcal{N}} g(V) \exp(-V/k_B T), \quad (14)$$

where  $\mathcal{N} = \int e^{-V/k_B T} g(V) dV$ . We hence calculate the average energy for the same systems we have explained above and reported in Fig. 3. Results are shown in Fig. 6. They qualitatively reproduce important features found in previous MD simulations [36] in which the energy of the FTS system transits from concave downwards at high temperature to concave upwards at low temperature. This feature is more pronounced when the energy is plotted against  $T$  as shown in the inset or when  $G_1$  is further reduced. In contrast, the energy of the fragile system remains concave downwards for the whole relevant temperature range.

#### IV. ONE-DIMENSIONAL MODEL

Our main simulations above have been performed in two dimensions. Many glassy features are believed to be independent of dimensions and previous two-dimensional (2D) simulations of the DPLM are able to reproduce qualitatively many characteristic properties of glass [24–29]. The DPLM has also demonstrated to behave qualitatively similarly in three dimensions [37]. To show that our results are independent of dimensions, we perform additional study in one dimension, which is computationally more efficient than in

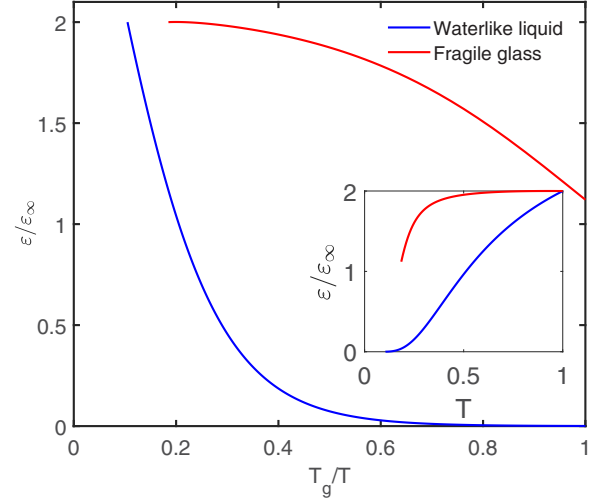


FIG. 6. The average energy per particle  $\varepsilon$  of the fragile system and the system with an FTS transition studied in Fig. 3 normalized by  $\varepsilon_\infty$ , which equals  $\varepsilon$  at the high-temperature limit. Inset:  $\varepsilon$  is plotted with the same data as in the main panel as a function of  $T$ .

two dimensions. In a truly one-dimensional (1D) lattice, particles cannot swap positions under the assumed void-induced dynamics and this can drastically alter the model characteristics. Our 1D model is therefore, more precisely, a quasi-1D model in which we shrink the width of the lattice in one direction and adopt a  $L \times 2$  lattice with  $L = 600$ . We apply periodic boundary conditions in both the long and short directions. Note that we keep taking  $C = 6$  in Eq. (9) as a hop attempt may involve either five or six bonds. Other parts of the algorithm are unchanged. This system allows particles to swap positions via a sequence of void-induced hops.

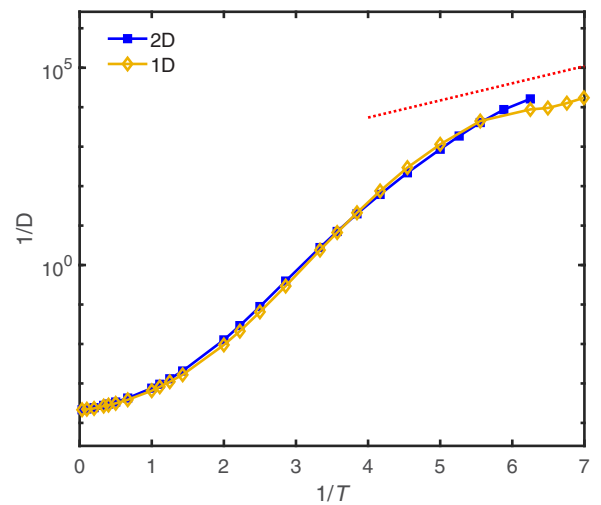


FIG. 7. An Arrhenius plot of  $1/D$  against  $1/T$  for a 1D model of waterlike liquid with  $G_1 = 0.15$ ,  $U_0 = 1.5$ ,  $w_0 = 6.7 \times 10^5$ , and  $\phi_v = 0.03$ . This is compared with results from Fig. 3 for a 2D model with  $G_1 = 0.38$ ,  $U_0 = 0.4$ ,  $w_0 = 10^4$ , and  $\phi_v = 0.01$ . In both cases, we take  $E_0 = 0$ . The dotted line following Eq. (11) is a guide to the eye.

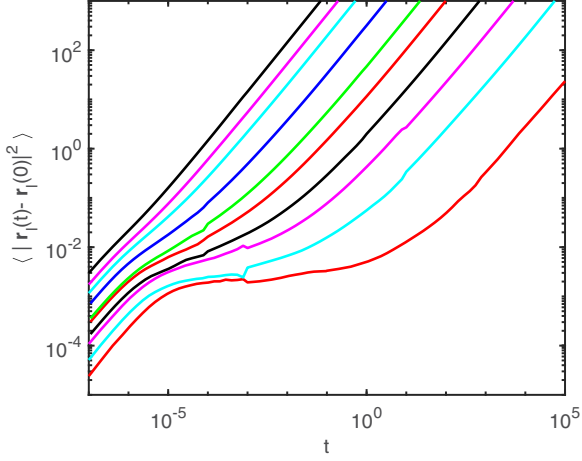


FIG. 8. MSD against  $t$  against time  $t$  for  $T = 3, 1, 0.7, 0.5, 0.4, 0.35, 0.3, 0.26, 0.22,$  and  $0.16$  (from left to right).

We consider  $G_1 = 0.15$  and  $w_0 = 6.7 \times 10^5$  so as to match the 2D results. We also increase the void density to  $\phi_v = 0.03$  from  $0.01$  so that average separation between voids is comparable to that in two dimensions. Figure 7 shows 1D results on  $1/D$  against  $1/T$ . Compared with 2D results reproduced from Fig. 3, much similarity is observed. A wider low-temperature Arrhenius regime below the FTS transition can now be observed in one dimension due to the better computational efficiency.

## V. DISCUSSIONS

As explained in Ref. [26], fragile glass can be simulated by the DPLM using the uniform-plus-delta pair-interaction distribution  $g(V)$  in Eq. (2) as shown in Fig. 3. Closely related to a two-state picture of glass [34], the two components in the distribution represent low-energy and high-energy states with average energies  $V_0 + k_B T$  and  $V_1$ , respectively. Glasses of the highest fragility are obtained when the weight  $G_0$  of

the low-energy state is small but nonvanishing. These low-energy interactions are thus rare and have a low entropy. As temperature decreases, interactions are increasingly restricted to these rare pairings, leading to a reduction of energetically favorable kinetic pathways and a dramatic slowdown of the dynamics. The low-energy component in  $g(V)$  in Eq. (2) has been approximated as a uniform distribution so that energy dispersion persists even when this component dominates at very low temperature. Super-Arrhenius behaviors thus persist to the lowest temperatures studied.

In this work, the fragile glass model is converted to a system with a FTS transition simply by replacing the lower uniform component of  $g(V)$  by a delta function at  $V_0$  in Eq. (4). At high temperature, such details in the lower component have little impact because the dynamics is dominated by whether individual interactions belong to the lower or the upper component. The fragile nature at high temperature is thus preserved. At low temperature when the lower-energy component dominates, the nondispersive energy at  $V_0$  results in the Arrhenius behavior of strong glass as shown in Eq. (11). This is consistent with the two-state scenario for liquid water, in which, as temperature decreases, the growth of the locally favored tetrahedral structure gives rise to the fragile behavior at high temperatures while its dominance at low temperatures leads to the Arrhenius behavior [11–14].

Although there has been much progress in studying fragile glass and amorphous systems with FTS transitions, their relations have been much less discussed. In particular, closely related two-state models [11–16,34] have found great success in their studies. Our lattice model approach allows studying both phenomena in a unified framework.

Lattice simulations are, in general, orders of magnitude faster than MD approaches. However, simulations at realistic timescales are still impossible and phenomena can often only be studied qualitatively at compressed timescales. Yet, we notice that the dynamics of our DPLM model shows the two characteristic turns in the Angell plot and the minimal stretching parameter  $\beta$ , in agreement with the FTS crossover in liquid water [11–14]. Despite its simplicity, the DPLM

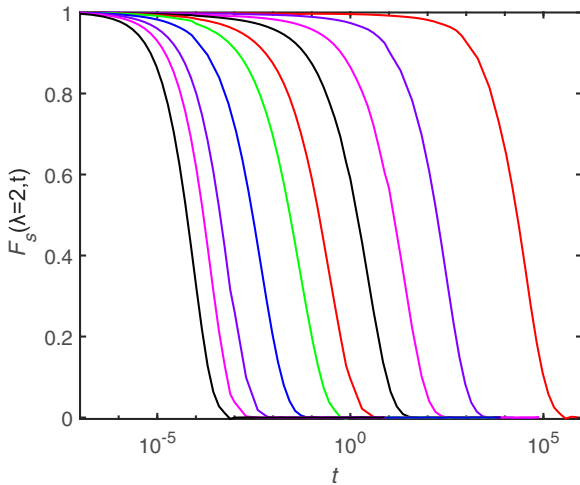


FIG. 9. Self-intermediate scattering function  $F_s(\mathbf{q}, t)$ , with  $|\mathbf{q}| = 2\pi/\lambda$  and  $\lambda = 2t$ , against time  $t$  for  $T = 3, 1, 0.7, 0.5, 0.4, 0.35, 0.3, 0.26, 0.22,$  and  $0.16$  (from left to right).

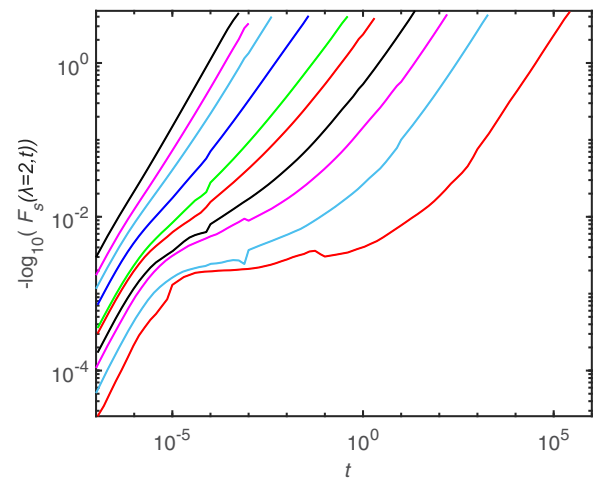
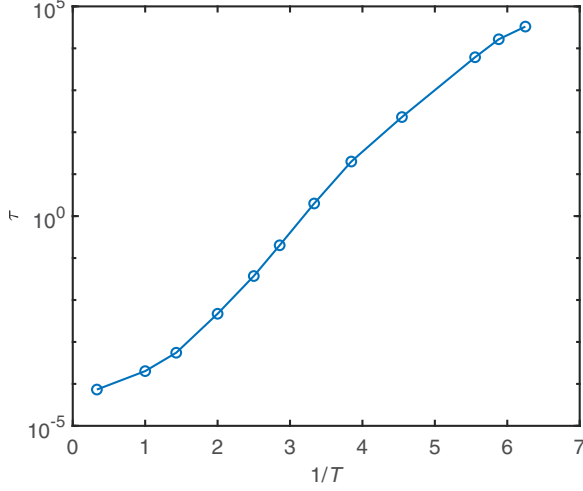


FIG. 10. Minus-log of self-intermediate scattering function against time  $t$  resulting in a log-log-versus-log plot using data from Fig. 9.

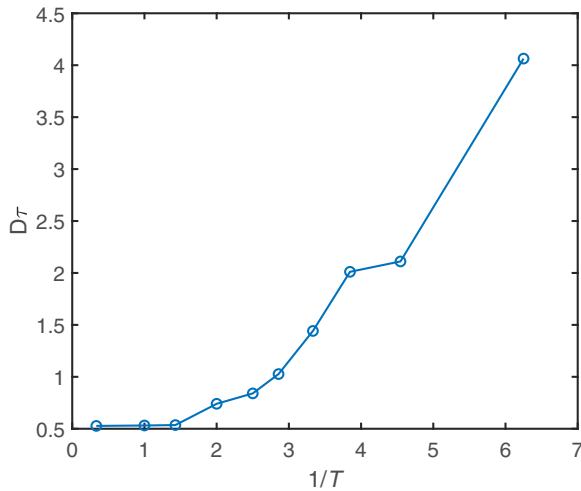
FIG. 11. Structural relaxation time  $\tau$  against  $T$ .

provides clear evidence supporting the two-state scenario for the FTS crossover in a lattice model of supercooled liquids.

To conclude, using a lattice model of glass, we have reproduced a FTS crossover separating a high-temperature fragile behavior from a low-temperature strong behavior. The model differs from that of fragile glass mainly by a different low-energy component of the pair-interaction energy distribution. While highly dispersed low-energy states lead to a fragile glass for the whole temperature range, a narrow low-energy distribution induces a FTS transition to a low-temperature strong regime. Our work provides a unified framework for studying fragile glass and systems exhibiting FTS transitions.

#### ACKNOWLEDGMENTS

This work was supported by the General Research Fund of Hong Kong (Grant No. 15303220), Shaanxi NSF Grant No.

FIG. 12. Plot of  $D\tau$  against  $T$ . The nonconstant values show a violation of the Stokes-Einstein relation.

2023-JC-QN-0018, and the National Natural Science Foundation of China (Grant No. 12175196).

#### APPENDIX: DETAILS OF DYNAMICAL CHARACTERIZATION

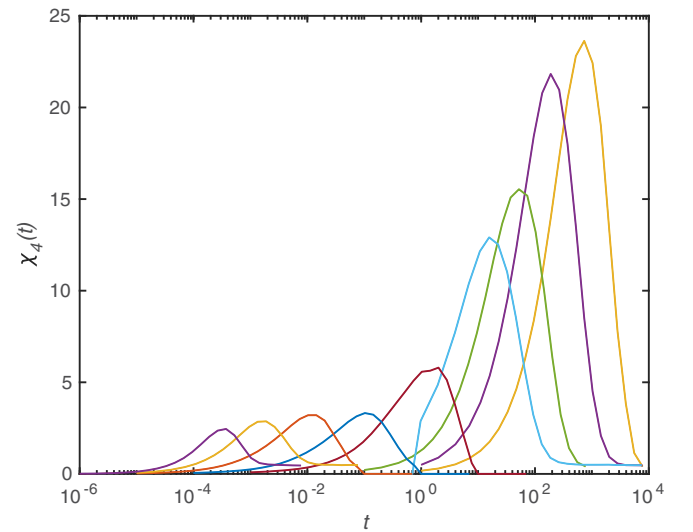
We now provide full details in the characterization of the dynamics of the DPLM with a bi-delta pair-interaction distribution,  $g(V)$ , in Eq. (4) which shows a FTS transition. We take the example of our 2D model of water introduced in Sec. III. Results for other parameters are qualitatively similar. As already explained, we adopt the probabilistic weight  $G_1 = 0.38$  of the low-energy component. Particle hops follow Eq. (8) with  $E_0 = 0$ ,  $w_0 = 10^6$ , and  $U_0 = 0.4$ . A void density of  $\phi_v = 0.01$  is used.

We have calculated the particle mean-square displacement (MSD) from  $\langle |\mathbf{r}_l(t) - \mathbf{r}_l(0)|^2 \rangle$ , with  $\mathbf{r}_l(t)$  denoting the position of particle  $l$  at time  $t$ . Figure 8 plots the MSD against time  $t$ . We observe the development of a plateau as temperature decreases. The particle diffusion coefficient  $D$  is then calculated from  $D = (1/2d)(\text{MSD}/t)$  at long time  $t$  and results are plotted in Fig. 3. Here,  $d = 2$  represents the dimension of the system. To ensure a sufficiently long time  $t$  in the calculation, only MSD values beyond 1 satisfying  $\text{MSD} \sim t^\gamma$  with  $\gamma \geq 0.96$  are considered.

Next, we examine the self-intermediate scattering function  $F_s$  defined as

$$F_s(\mathbf{q}, t) = \langle e^{i\mathbf{q} \cdot [\mathbf{r}_l(t) - \mathbf{r}_l(0)]} \rangle, \quad (\text{A1})$$

where  $|\mathbf{q}| = 2\pi/\lambda$  with  $\lambda = 2$ . Figure 9 plots  $F_s$  against  $t$ . It shows a two-step relaxation with a tiny first step. The main relaxation in  $F_s$  follows the Kohlrausch-Williams-Watts stretched exponential function  $A \exp[-(t/\tau)^\beta]$ , where  $\beta$  is the stretching exponent,  $\tau$  is the relaxation time, and  $A$  is a

FIG. 13. Four-point correlation function  $\chi_4(t)$  against time  $t$  for  $T = 1, 0.6, 0.45, 0.35, 0.3, 0.26, 0.24, 0.22$ , and  $0.20$  (from left to right).

constant close to 1. We plot  $-\log(F_s)$  against  $t$  in log-log scales in Fig. 10 from which we obtain  $\beta$  for different  $T$  by computing the slope of the linear region at large  $t$  satisfying  $10^{-3} \leq F_s(\mathbf{q}, t) \leq 0.9$ . Results on  $\beta$  are shown in Fig. 4. The relaxation time  $\tau$  can be obtained as the time at which  $F_s = 1/e$ . In Fig. 11, we plot  $\tau$  against  $1/T$ . Figure 12 then further shows a violation in the Stokes-Einstein relation as observed from an increase of  $D\tau$  when  $T$  decreases. We have also studied the four-point correlation function defined by

$\chi_4 = N \langle (O(t) - \bar{O}(t))^2 \rangle$ , in which

$$O(t) = \frac{1}{N} \Theta[|\mathbf{r}_i(t) - \mathbf{r}_i(0)|], \quad (\text{A2})$$

where  $\Theta(\mathbf{r})$  is the Heaviside step function. Figure 13 plots  $\chi_4(t)$  against time  $t$  for various  $T$ . We observe that  $\chi_4(t)$  maximizes at the dynamical timescale  $\tau_4$ . The peak height  $\chi_4(\tau_4)$  is plotted against  $T$  in Fig. 5.

- 
- [1] F. H. Stillinger and P. G. Debenedetti, Glass transition thermodynamics and kinetics, *Annu. Rev. Condens. Matter Phys.* **4**, 263 (2013).
- [2] G. Biroli and J. P. Garrahan, Perspective: The glass transition, *J. Chem. Phys.* **138**, 12A301 (2013).
- [3] F. Arceri, F. P. Landes, L. Berthier, and G. Biroli, Glasses and aging: A statistical mechanics perspective, *Statistical and Nonlinear Physics* (Springer, 2022) p. 229.
- [4] K. Ito, C. T. Moynihan, and C. A. Angell, Thermodynamic determination of fragility in liquids and a fragile-to-strong liquid transition in water, *Nature (London)* **398**, 492 (1999).
- [5] C. A. Angell, Water II is a “strong” liquid, *J. Phys. Chem.* **97**, 6339 (1993).
- [6] A. Saksengwijit, J. Reinisch, and A. Heuer, Origin of the fragile-to-strong crossover in liquid silica as expressed by its potential-energy landscape, *Phys. Rev. Lett.* **93**, 235701 (2004).
- [7] M. Hemmati, C. T. Moynihan, and C. A. Angell, Interpretation of the molten BeF<sub>2</sub> viscosity anomaly in terms of a high temperature density maximum, and other waterlike features, *J. Chem. Phys.* **115**, 6663 (2001).
- [8] Z. Evenson, T. Schmitt, M. Nicola, I. Gallino, and R. Busch, High temperature melt viscosity and fragile to strong transition in Zr–Cu–Ni–Al–Nb(Ti) and Cu<sub>47</sub>Ti<sub>34</sub>Zr<sub>11</sub>Ni<sub>8</sub> bulk metallic glasses, *Acta Mater.* **60**, 4712 (2012).
- [9] P. Gallo, M. Rovere, and E. Spohr, Supercooled confined water and the mode coupling crossover temperature, *Phys. Rev. Lett.* **85**, 4317 (2000).
- [10] L. Xu, P. Kumar, S. V. Buldyrev, S.-H. Chen, P. H. Poole, F. Sciortino, and H. E. Stanley, Relation between the Widom line and the dynamic crossover in systems with a liquid–liquid phase transition, *Proc. Natl. Acad. Sci. USA* **102**, 16558 (2005).
- [11] R. Shi, J. Russo, and H. Tanaka, Common microscopic structural origin for water’s thermodynamic and dynamic anomalies, *J. Chem. Phys.* **149**, 224502 (2018).
- [12] R. Shi, J. Russo, and H. Tanaka, Origin of the emergent fragile-to-strong transition in supercooled water, *Proc. Natl. Acad. Sci. USA* **115**, 9444 (2018).
- [13] R. Shi and H. Tanaka, The anomalies and criticality of liquid water, *Proc. Natl. Acad. Sci. USA* **117**, 26591 (2020).
- [14] Z. Yu, R. Shi, and H. Tanaka, A unified description of the liquid structure, static and dynamic anomalies, and criticality of TIP4P/2005 water by a hierarchical two-state model, *J. Phys. Chem. B* **127**, 3452 (2023).
- [15] H. Tanaka, Simple physical model of liquid water, *J. Chem. Phys.* **112**, 799 (2000).
- [16] H. Tanaka, A new scenario of the apparent fragile-to-strong transition in tetrahedral liquids: Water as an example, *J. Phys.: Condens. Matter* **15**, L703 (2003).
- [17] G. E. Walrafen, Raman spectral studies of the effects of temperature on water structure, *J. Chem. Phys.* **47**, 114 (1967).
- [18] G. E. Walrafen, M. R. Fisher, M. S. Hokmabadi, and W.-H. Yang, Temperature dependence of the low- and high-frequency Raman scattering from liquid water, *J. Chem. Phys.* **85**, 6970 (1986).
- [19] A. S. Woutersen, U. Emmerichs, and H. J. Bakker, Femtosecond mid-IR pump-probe spectroscopy of liquid water: Evidence for a two-component structure, *Science* **278**, 658 (1997).
- [20] A. Taschin, P. Bartolini, R. Eramo, R. Righini, and R. Torre, Evidence of two distinct local structures of water from ambient to supercooled conditions, *Nat. Commun.* **4**, 2401 (2013).
- [21] R. Shi and H. Tanaka, Direct evidence in the scattering function for the coexistence of two types of local structures in liquid water, *J. Am. Chem. Soc.* **142**, 2868 (2020).
- [22] C. De Michele, P. Tartaglia, and F. Sciortino, Slow dynamics in a primitive tetrahedral network model, *J. Chem. Phys.* **125**, 204710 (2006).
- [23] C. De Michele, S. Gabrielli, P. Tartaglia, and F. Sciortino, Dynamics in the presence of attractive patchy interactions, *J. Phys. Chem. B* **110**, 8064 (2006).
- [24] L.-H. Zhang and C.-H. Lam, Emergent facilitation behavior in a distinguishable-particle lattice model of glass, *Phys. Rev. B* **95**, 184202 (2017).
- [25] M. Lulli, C.-S. Lee, H.-Y. Deng, C.-T. Yip, and C.-H. Lam, Spatial heterogeneities in structural temperature cause Kovacs’ expansion gap paradox in aging of glasses, *Phys. Rev. Lett.* **124**, 095501 (2020).
- [26] C.-S. Lee, M. Lulli, L.-H. Zhang, H.-Y. Deng, and C.-H. Lam, Fragile glasses associated with a dramatic drop of entropy under supercooling, *Phys. Rev. Lett.* **125**, 265703 (2020).
- [27] C.-S. Lee, H.-Y. Deng, C.-T. Yip, and C.-H. Lam, Large heat-capacity jump in cooling-heating of fragile glass from kinetic Monte Carlo simulations based on a two-state picture, *Phys. Rev. E* **104**, 024131 (2021).
- [28] X.-Y. Gao, H.-Y. Deng, C.-S. Lee, J. You, and C.-H. Lam, Emergence of two-level systems in glass formers: a kinetic Monte Carlo study, *Soft Matter* **18**, 2211 (2022).
- [29] G. Gopinath, C.-S. Lee, X.-Y. Gao, X.-D. An, C.-H. Chan, C.-T. Yip, H.-Y. Deng, and C.-H. Lam, Diffusion-coefficient power laws and defect-driven glassy dynamics in swap acceleration, *Phys. Rev. Lett.* **129**, 168002 (2022).
- [30] C.-H. Chan, Q. Huo, A. Kumar, Y. Shi, H. Hong, Y. Du, S. Ren, K.-P. Wong, and C.-T. Yip, Heterogeneity and memory effect in the sluggish dynamics of vacancy defects in colloidal disordered crystals and their implications to high-entropy alloys, *Adv. Sci.* **9**, 2205522 (2022).



- [31] C.-H. Lam, Local random configuration-tree theory for string repetition and facilitated dynamics of glass, *J. Stat. Mech.* (2018) 023301.
- [32] J. T. Titantah and M. Karttunen, Water dynamics: Relation between hydrogen bond bifurcations, molecular jumps, local density & hydrophobicity, *Sci. Rep.* **3**, 2991 (2013).
- [33] P. G. Debenedetti, Supercooled and glassy water, *J. Phys.: Condens. Matter* **15**, R1669 (2003).
- [34] C. T. Moynihan and C. A. Angell, Bond lattice or excitation model analysis of the configurational entropy of molecular liquids, *J. Non-Cryst. Solids* **274**, 131 (2000).
- [35] H.-Y. Deng, C.-S. Lee, M. Lulli, L.-H. Zhang, and C.-H. Lam, Configuration-tree theoretical calculation of the mean-squared displacement of particles in glass formers, *J. Stat. Mech.* (2019) 094014.
- [36] I. Saika-Voivod, P. H. Poole, and F. Sciortino, Fragile-to-strong transition and polyamorphism in the energy landscape of liquid silica, *Nature (London)* **412**, 514 (2001).
- [37] B. Li, C.-S. Lee, X.-Y. Gao, H.-Y. Deng, and C.-H. Lam, The distinguishable-particle lattice model of glasses in three dimensions, *Soft Matter* **20**, 1009 (2024).